

Supplementary Information

Selectivity Enhancement in Electrochemical Reduction of Oxalic Acid on Titanium Dioxide Nanoparticles Achieved by Shape and Energy States Controls

Hiroto Eguchi^a, Kenichi Kato^b, Gergely Juhász^{c,*} & Miho Yamauchi^{a,d,e*}

*Correspondence to yamauchi@i2cner.kyushu-u.ac.jp, juhasz.g.aa@m.titech.ac.jp

a Department of Chemistry, Graduate School of Science, Kyushu University, 744
Motooka, Nishi-ku Fukuoka 819-0395, Japan.

b RIKEN SPring-8 Center, 1-1-1 Kouto, Sayo-cho, Sayo-gun, Hyogo, 679-5148, Japan.

c Department of Chemistry, Graduate School of Science, Tokyo Institute of
Technology, 2-12-1 Ookayama, Meguro-ku, Tokyo, 152-8550, Japan.

d International Institute for Carbon-Neutral Energy Research (WPI-I²CNER), Kyushu
University, 744 Motooka, Nishi-ku Fukuoka 819-0395, Japan.

e Advanced Institute for Materials Research(AIMR), Tohoku University, 2-1-1
Katahira, Aoba-ku, Sendai, 980-8577, Japan

Materials and Methods

Materials

Ammonium chloride (99.5%), 2-propanol (99.7%), tetrabutyl orthotitanate (95%), sulfuric acid (95%), acetic acid (99.7%), N,N-dimethylformamide (99%), oxalic acid (98%) and sodium sulfate (99%) were purchased from Wako. Ammonium Fluoride (97%) and diethylenetriamine (97%) were purchased from Kanto Chemical Co., Inc. Tetraisopropyl orthotitanate (95%) and ammonia solution (28%) were purchased from nacalai tesque. Titanium foil (99.5%) was purchased from Nilaco. All chemicals were used without further purification.

Synthesis of TiO₂ NPs

TiO₂ nanoparticles (NPs) of a columnar truncated bipyramidal decahedron exposed {101} facets (101-column) were synthesized according to previously reported solvothermal synthesis.¹ In a typical experiment, 0.8 g of NH₄Cl was added into 8 mL 2-propanol, then stirred for about 5 min. After stirring, 0.2 mL of tetraisopropyl orthotitanate was dropped in the mixed solution, then stirred for about 30 min. Next, 10 mL of NH₃ (28%) aqueous solution was dropped into the mixed solution, and the mixture was stirred for about 5min. The solution was transferred into a 60 mL Teflon-lined stainless steel autoclave. The autoclave was sealed and heated in an oven at 170 °C for 72 h. After reactions, a white product was washed and centrifuged with deionized water and acetone, and then dried under vacuum.

TiO₂ NPs of a truncated bipyramidal decahedron exposed {101} facets (101-deca) were synthesized according to previously reported hydrothermal synthesis.^{2,3} In a typical experiment, 1 mL of tetrabutyl orthotitanate was added into 30 mL deionized water, then stirred for about 30 min. After stirring, the solution was transferred into a 60 mL Teflon-lined stainless steel autoclave. The autoclave was sealed and heated in an oven at 200 °C

for 24 h. After reactions, a white product was washed and centrifuged with deionized water and acetone, and then dried under vacuum.

TiO₂ NPs of a truncated bipyramidal decahedron exposed {001} facets (001-deca) were synthesized according to previously reported hydrothermal synthesis.^{3,4} In a typical experiment, 0.65 g of NH₄F was added into 35 mL deionized water, then stirred. 1 mL of tetraisopropyl orthotitanate was dropped in the mixed solution, then stirred for about 30 min. The solution was transferred into a 60 mL Teflon-lined stainless steel autoclave. The autoclave was sealed and heated in an oven at 200 °C for 24 h. After reactions, a white product was washed and centrifuged with deionized water and acetone, and then dried under vacuum.

TiO₂ NPs of a sphere condensed sheet exposed {001} facets (001-sheet-C) were synthesized according to previously reported solvothermal synthesis.⁵ In a typical experiment, 0.03 mL of diethylenetriamine was added into 42 mL 2-propanol, then stirred for about 5 min. After stirring, 1.5 mL of tetraisopropyl orthotitanate was dropped in the mixed solution. The solution was transferred into a 60 mL Teflon-lined stainless steel autoclave. The autoclave was sealed and heated in an oven at 200 °C for 24 h. After reactions, a white product was washed and centrifuged with deionized water and ethanol, and then dried under vacuum. After drying, the product was calcined at 400 °C for 2 h.

TiO₂ NPs of a sphere stacked sheet exposed {001} facets (001-sheet-S) were synthesized according to previously reported solvothermal synthesis.⁶ In a typical experiment, 6.6 mL of sulfuric acid was added into 53 mL deionized water. Next, 1 mL of tetrabutyl orthotitanate was dropped in the mixed solution, then stirred for about 30 min. 30 mL of mixed solution was transferred into a 60 mL Teflon-lined stainless steel autoclave. The autoclave was sealed and heated in an oven at 180 °C for 5 h. After reactions, a white product was washed and filtrated with deionized water, and then dried under vacuum.

TiO₂ NPs of truncated asymmetric bipyramidal decahedron exposed {201} facets (201-deca) were synthesized according to previously reported solvothermal synthesis.⁷ In a typical experiment, 32 mL of acetic acid was added into 47 mL N,N-dimethylformamide, then stirred. After stirring, 0.5 mL of tetrabutyl orthotitanate was dropped into 20 mL of mixed solution. The solution was transferred into a 60 mL Teflon-lined stainless steel autoclave. The autoclave was sealed and heated in an oven at 200°C for 10 h. After reactions, a white product was washed and centrifuged with ethanol, and then dried under vacuum.

Sample characterization

X-ray diffraction (XRD) measurements were conducted using BL44B2, SPring-8 with $\lambda = 0.5005 \text{ \AA}$.^{8,9} Transmission electron microscope (TEM) images were collected on a JEM-2100HCKM (JEOL) operated at 200 kV. Sample grids for the TEM observations were prepared by dropping methanol dispersions of the samples onto a carbon grid. Scanning electron microscope (SEM) observations were conducted on an SU9000 (HITACHI). Samples were attached to the double-sided carbon tape. Ultraviolet visible absorption (UV-vis) spectra were collected using a V670 spectrometer (JASCO). The diffuse reflection spectra were transformed using the Kubelka-Munk function. Nitrogen adsorption-desorption measurements were performed at -196 °C on a BELSORP-max (Bel Japan). Prepared Samples were degassed at 100 °C under vacuum. Alternating current (AC) impedance measurement was carried out using a SI1260/SI1296 (solartron). The sample was pressed to a pellet and the pellet was pasted gold with gold wire. The X-ray photoelectron spectroscopy (XPS) spectra were recorded on a VersaProbeII (ULVAC-PHI) with Al anode X-ray source. All the binding energies were referenced to the peak of C 1s binding energy at 284.6 eV. The ultraviolet photoelectron spectroscopy (UPS) spectra were recorded on a VersaProbeII (ULVAC-PHI) with He I source.

Electrochemical measurement and product analysis

Working electrodes were prepared according to previously reported procedure.^{10, 11} Ti foils ($2 \times 2.5 \text{ cm}^2$) were calcined at $450 \text{ }^\circ\text{C}$ for 1 h under air atmosphere. After calcination, methanol (0.2 mL) dispersions of the TiO_2 catalyst (10 mg) dropped onto the calcined Ti foils. The TiO_2 catalyst loading Ti foil was calcined at $500 \text{ }^\circ\text{C}$ for 1 h under air atmosphere.

Cyclic voltammetry (CV) measurements were performed by a three-electrode system connected to a VersaSTAT4 potentiostat (AMETEC, Princeton Applied Research). The TiO_2 catalyst loading Ti foil, coiled Pt wire and Ag/AgCl were used as the working electrode, counter electrode, and reference electrode respectively. An electrolyte aqueous solution (80 mL of 0.03 M oxalic acid and 0.2 M Na_2SO_4) was placed into a glass cell. The electrolyte was bubbled with Ar gas for 30 min in order to purge the air. The CV measurement was carried out at $50 \text{ }^\circ\text{C}$. The CV measurement for a blank solution (80 mL of 0.2 M Na_2SO_4) was performed following the same procedures. The current density was calculated by the surface area of the electrode. The iR correction was not performed and the reference electrode was not calibrated to the temperature.

Tafel plots for electrochemical reaction on TiO_2 NPs were obtained by using a three-electrode system connected to a VersaSTAT4 potentiostat (AMETEC, Princeton Applied Research). The TiO_2 catalyst loading Ti foil, coiled Pt wire and Ag/AgCl were used as the working electrode, counter electrode, and reference electrode, respectively. An electrolyte aqueous solution (80 mL of 0.03 M oxalic acid and 0.2 M Na_2SO_4) was placed into a glass cell. The electrolyte was bubbled with Ar gas for 30 min in order to purge the air. The polarization curves were obtained by a slow linear sweep of 0.5 mV s^{-1} . The iR correction was not performed and the reference electrode was not calibrated to the temperature.

Chronoamperometry (CA) measurements were conducted according to previously reported standard condition.^{10,11} CA measurements were performed in a three-electrode system connected to a VersaSTAT4 potentiostat (AMETEC, Princeton Applied Research) with two-compartment glass cell. The TiO₂ catalyst loading Ti foil, coiled Pt wire and Ag/AgCl were used as a working electrode, counter electrode, and reference electrode respectively. The proton-conducting membrane (Nafion® , NRE-212, Sigma-Aldrich) was used as a separator to prevent exchanging reactant. An electrolyte aqueous solution (40 mL of 0.03 M oxalic acid and 0.2 M Na₂SO₄), the working electrode and the reference electrode were placed into the cathodic cell. An electrolyte aqueous solution (40 mL of 0.2 M Na₂SO₄), the reference electrode were placed into the anodic cell. The pH values of the solution were adjusted 2.1 by H₂SO₄ addition. The electrolyte was bubbled with Ar gas for 30 min in order to purge the air. The CA measurement was carried out at -0.7 V vs. RHE and 50 °C for 2 hours. The iR correction was not performed and the reference electrode was not calibrated to the temperature. The reaction products in the cathodic cell were analyzed using a high-performance liquid chromatograph (LC-20AD, Shimadzu). The gaseous reaction products in the cathodic cell were investigated using a gas chromatography (GC-8A, Shimadzu).

The Faradaic yield in the electroreduction measurements is defined as following formula.

$$\text{Faradaic yield}(\%) = \frac{m_{\text{products}} \times n \times F}{Q} \times 100$$

Here m_{products} is the moles of electroreduction products. n is the number of electrons required for a reaction of starting materials to products. The electroreduction of oxalic acid to glyoxylic acid is required two electrons ($n = 2$) and to glycolic acid is required four electrons ($n = 4$). The electroreduction of H⁺ to H₂ is needed two electrons ($n = 2$). F is Faraday constant (96,485 C mol⁻¹). Q is the total charge in the reaction.

Calculations

The calculations were performed with Density-Functional based Tight-Binding (DFTB-SCF) method as implemented in DFTB+ software (ver. 1.2).^{12,13} We used tio-0-1 and mio-0-1 parameter sets¹⁴ and a convergence criteria of 10^{-5} a.u. for SCF cycles, and 10^{-3} a.u. for the geometry optimization.

Surface absorption models were created on three TiO₂ layers thick anatase slabs with (101) and (001) surfaces. The vacuum layer between the anatase slabs were at least 20Å. Solvent effects were not considered. The absorbed molecules and the slab geometry were optimized whereas the cell parameters and bottom TiO₂ layer of the slab were kept constrained. The k-points for the integration of the Brillouin zone at 2x4x1 were chosen using Monkhorst-Pack sampling¹⁵. The optimized lowest energy geometries of oxalate on the (101) and (001) surfaces are shown in Figure S1.

Nanoparticle models **NP 1**, **2** and **3** (see Figure S2) were chosen to simulate the behavior of nanoparticles with dominantly (101) and (001) surfaces, and closest to regular, 101-column, 101-deca, 001-deca nanoparticle shapes. The models were cut out from bulk anatase lattice along the relevant Miller planes, and Ti atoms with low coordination were capped with –OH groups to reach charge neutrality, and the lowest energy isomer were chosen. The size of nanoparticle models is between 3.5-4.5 nm. All the models were optimized without any symmetry or geometry constraints.

The distribution of the extra electron on the reduced nanoparticle (Δ^-) and the hole on the oxidized nanoparticle (Δ^+) (“extra charges”) were calculated as the difference of electron density (see Figure S3 and S4) and Mulliken charges between the charged (–1) and the corresponding neutral nanoparticles.

$$\Delta^- = \rho_{-1} - \rho_0$$

$$\Delta+ = \rho_{+1} - \rho_0$$

The geometries of the charged nanoparticles were kept the same as the neutral one, which cause no significant error but simplifies the comparison.

The absorption on oxalic acid molecules on the nanoparticles were studied by manually inserting the molecule on different positions of nanoparticle (see in Figure S5), and relaxing the geometry without any constrains. All the most stable geometries were dissociative type similar to the geometries observed on simple surface models. Due to the large calculation cost, we focused to **NP 1** and **3** (preliminary calculations showed that **NP 2** behaves similar way to 1).

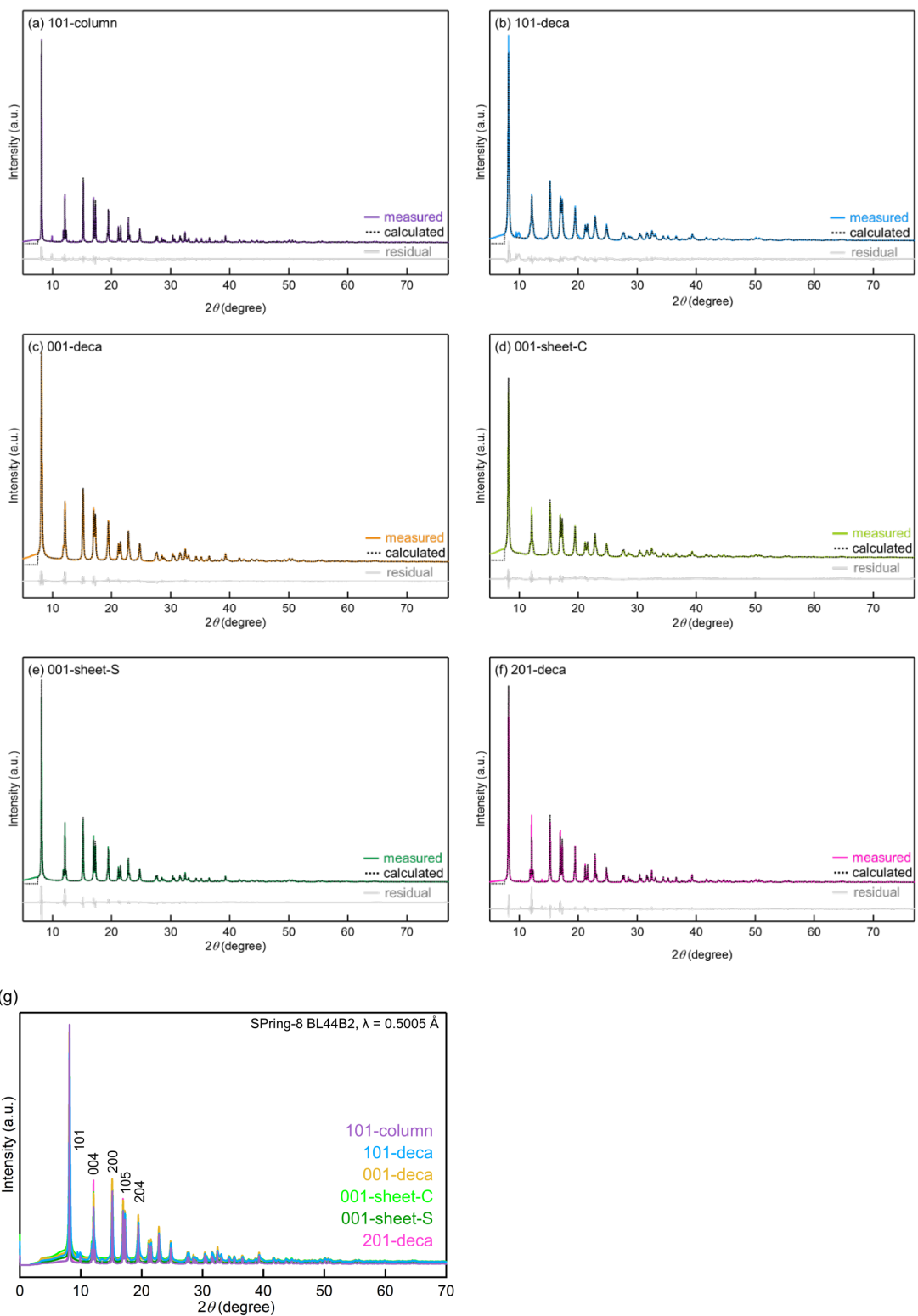


Figure S1 Rietveld analysis results for XRD pattern for TiO₂ NPs: (a) 101-column, (b) 101-deca, (c) 001-deca, (d) 001-sheet-C, (e) 001-sheet-S, (f) 201-deca. (g) XRD patterns of the TiO₂ NPs prepared by solvothermal synthesis.

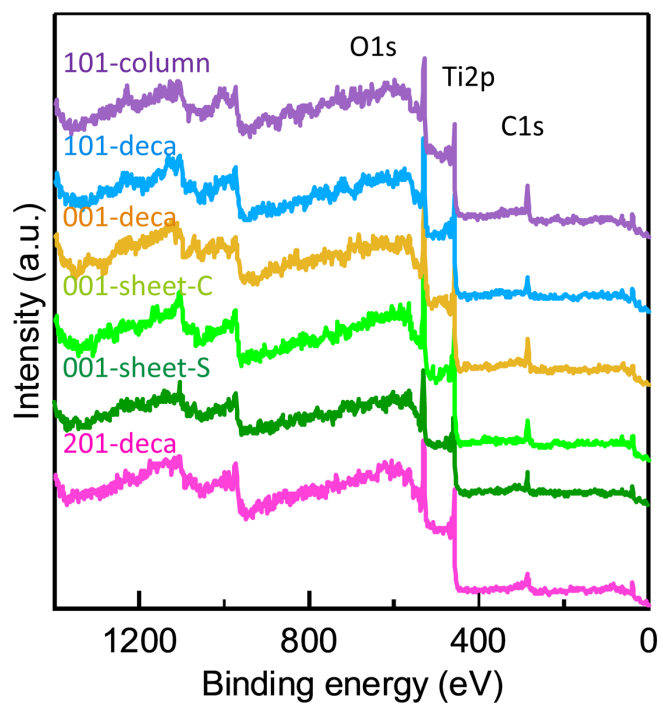


Figure S2 XPS survey spectra of TiO₂ NPs.

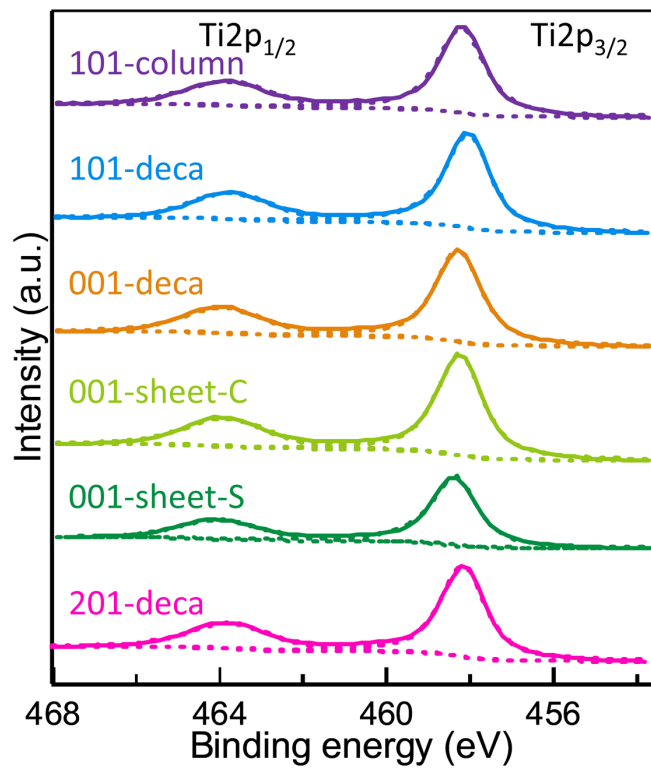


Figure S3 Ti2p XPS spectra of TiO₂ NPs.

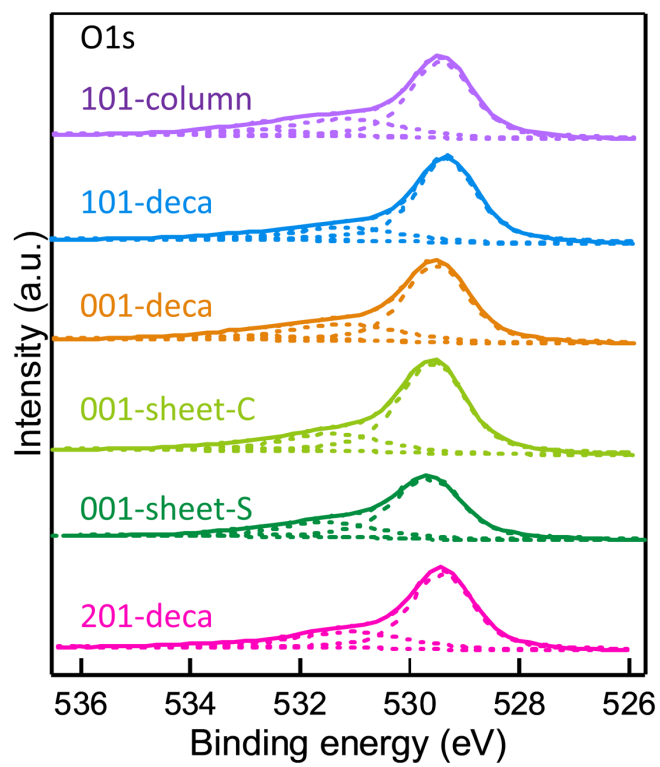


Figure S4 O1s XPS spectra of TiO₂ NPs.

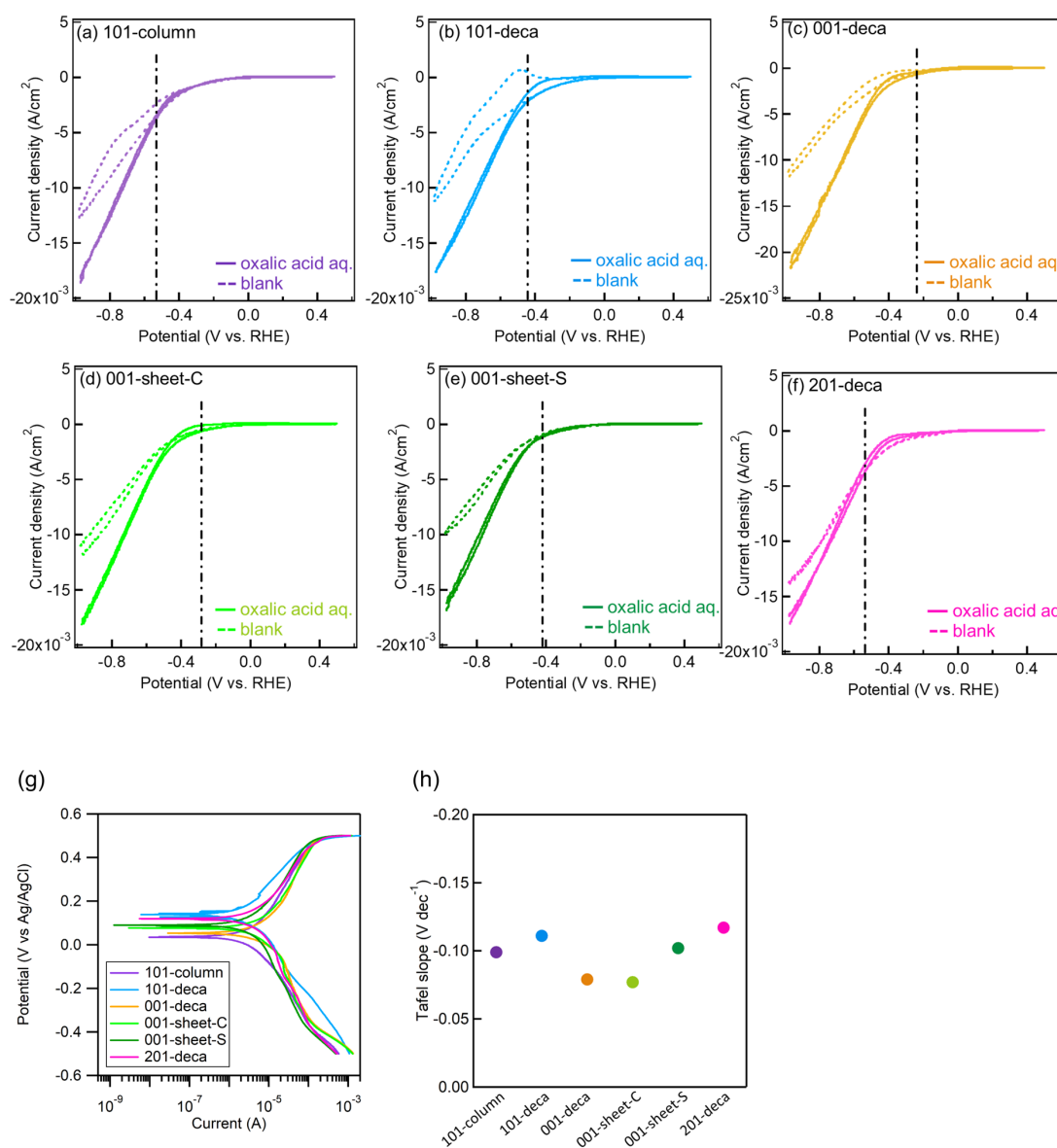


Figure S5 Cyclic voltammograms for the electrochemical reduction of oxalic acid on TiO₂ NPs: (a) 101-column, (b) 101-deca, (c) 001-deca, (d) 001-sheet-C, (e) 001-sheet-S, (f) 201-deca. The black dashed line indicates the onset potential. The current density was calculated by the surface area of the electrode. (g) Tafel plots for electrochemical reduction of oxalic acid on TiO₂ NPs. (h) Tafel slopes estimated from the Tafel plot (g) between -0.2 and -0.5 V vs. Ag/AgCl.

We produced Tafel plots to deepen our understanding for the electrochemical reduction of oxalic acid. Figure S10(g) shows the Tafel plot for TiO₂ NPs. We can find tiny steps

in the Tafel plot between -0.2 and -0.5 V vs. Ag/AgCl. Therefore, we think that the Tafel plots are composed of multiple elementary reactions including hydrogen evolution. Then, averaged Tafel slopes were estimated using the data in the potential region from -0.2 to -0.5 V vs. Ag/AgCl and are shown in Figure S5(h). We cannot see obvious differences among Tafel slopes, which suggests that several reaction steps are complicatedly reflected in the Tafel plot for TiO_2 catalysts prepared in this study.

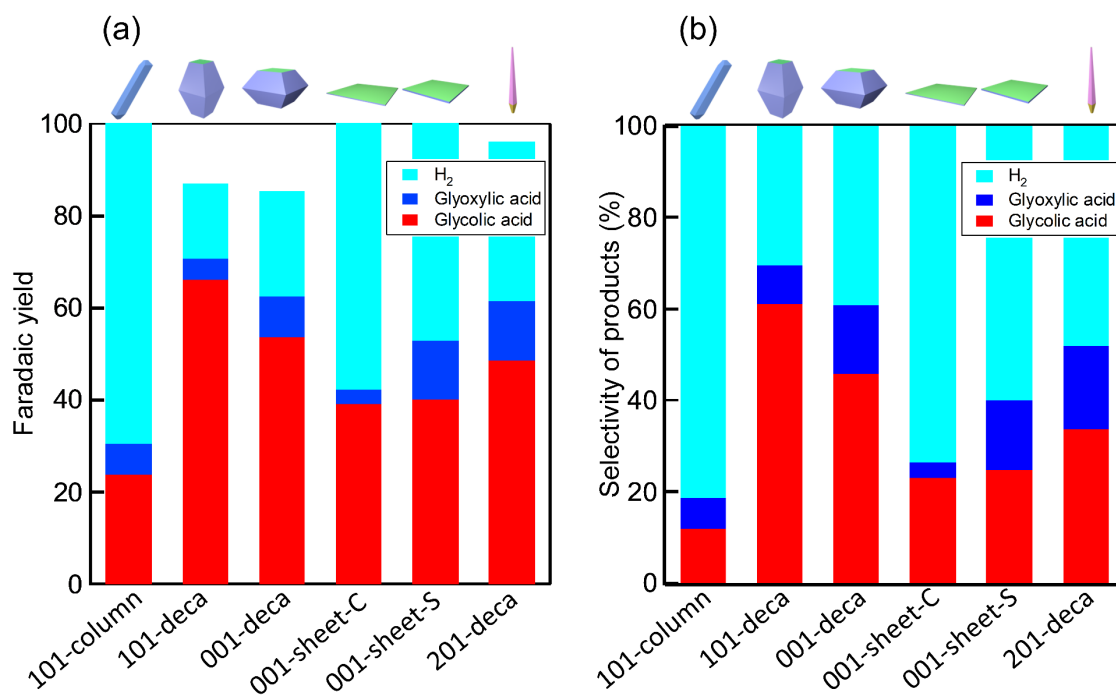


Figure S6 (a) Faradaic yield and (b) selectivity for electrochemical reduction of oxalic acid on TiO₂ NPs.

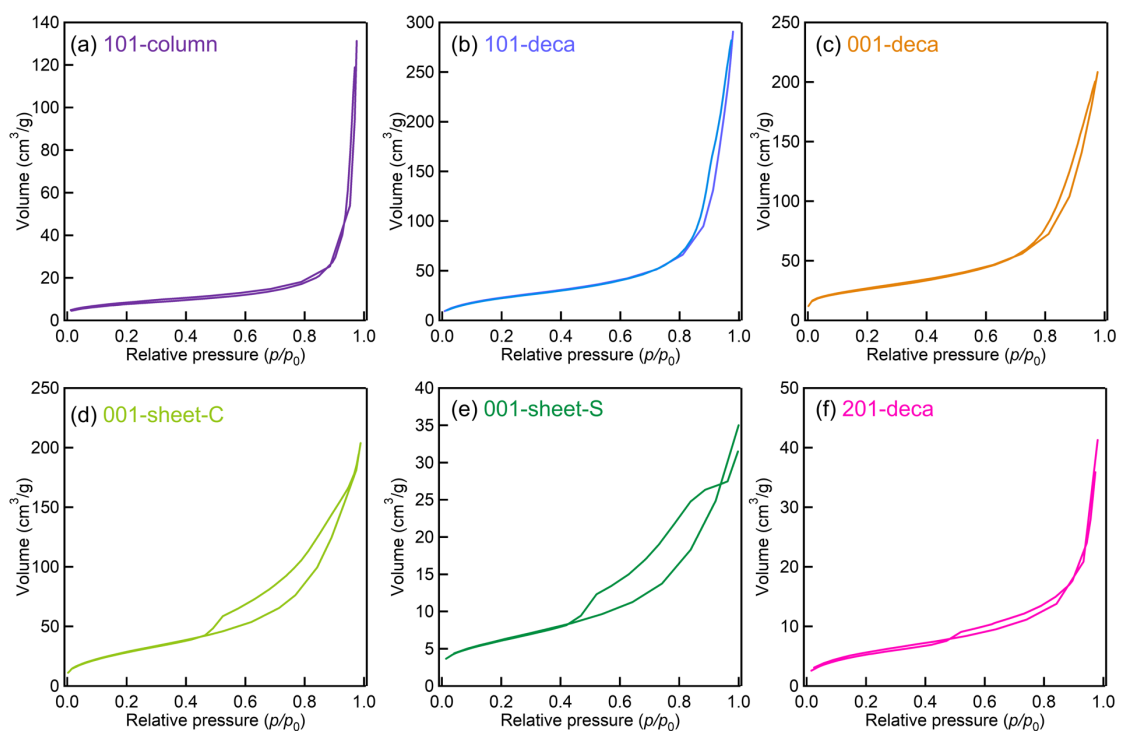


Figure S7 The nitrogen adsorption-desorption curves on TiO₂NPs: (a) 101-column, (b) 101-deca, (c) 001-deca, (d) 001-sheet-C, (e) 001-sheet-S, (f) 201-deca.

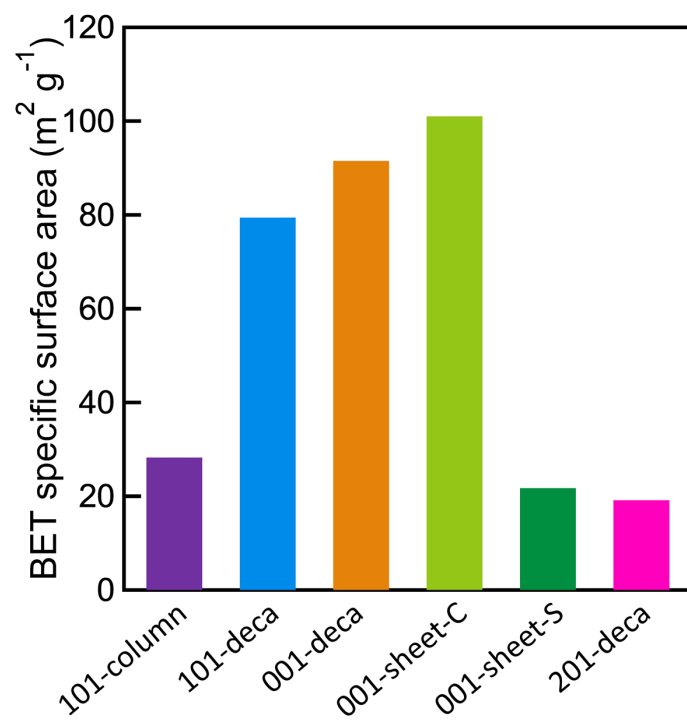


Figure S8 BET specific surface area of TiO₂ NPs.

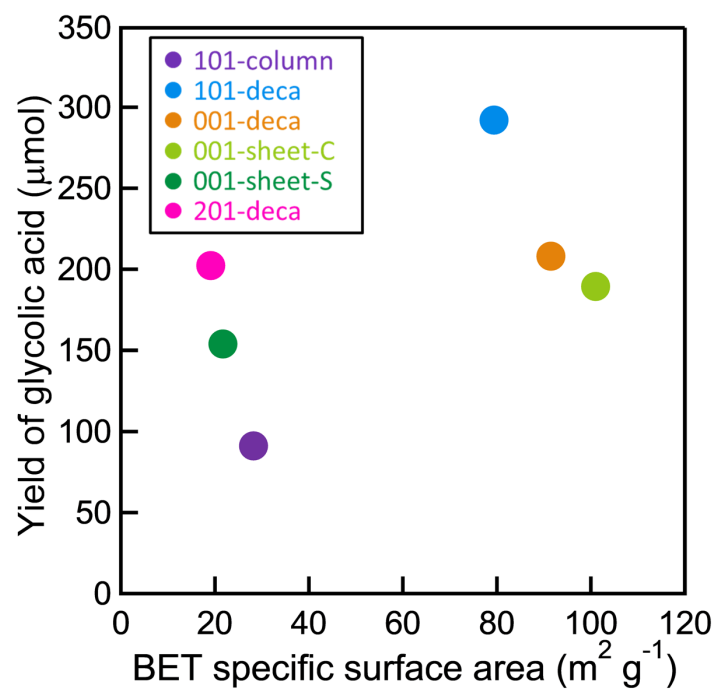


Figure S9 The relationship between BET specific surface area of TiO_2 NPs and the yields of glycolic acid (GC).

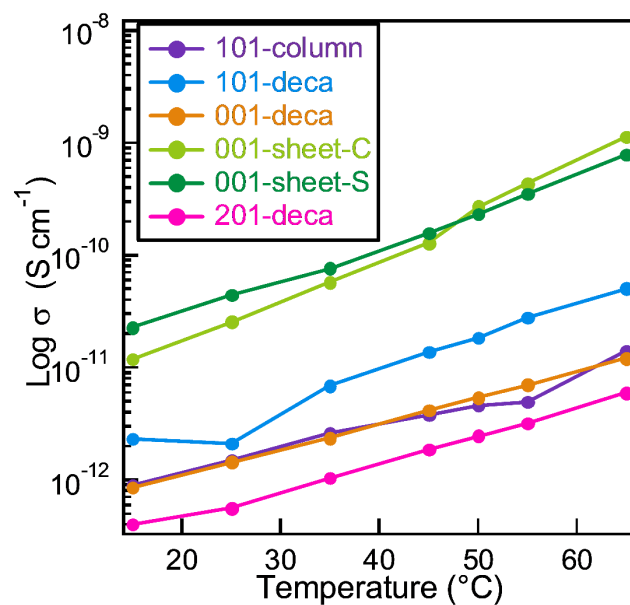


Figure S10 The temperature dependence of electronic conductivity of TiO₂ NPs.

We found that TiO₂ NPs have electronic conductivity in the range from 10⁻⁹ to 10⁻¹² S cm⁻¹ at 50 °C, which is similar to those reported for TiO₂ samples and the electronic conductivity strongly depends on the shape of TiO₂ NPs.

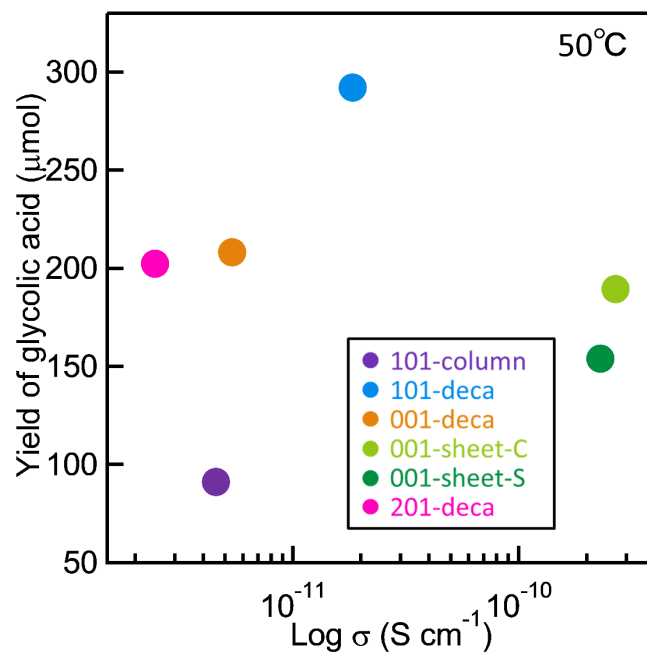


Figure S11 The relationship between the yields of glycolic acid (GC) and the electronic conductivity of TiO_2 NPs.

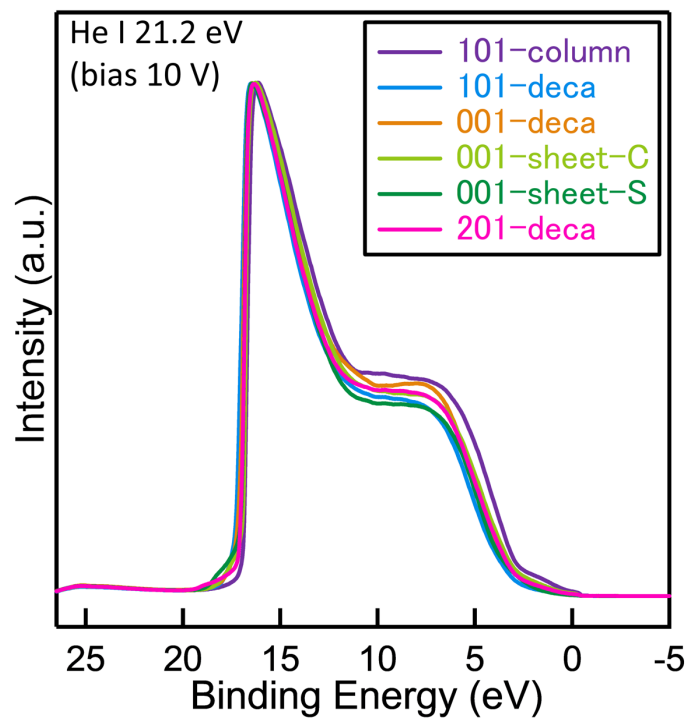


Figure S12 Ultraviolet photoelectron spectroscopy (UPS) spectra of TiO₂ NPs.

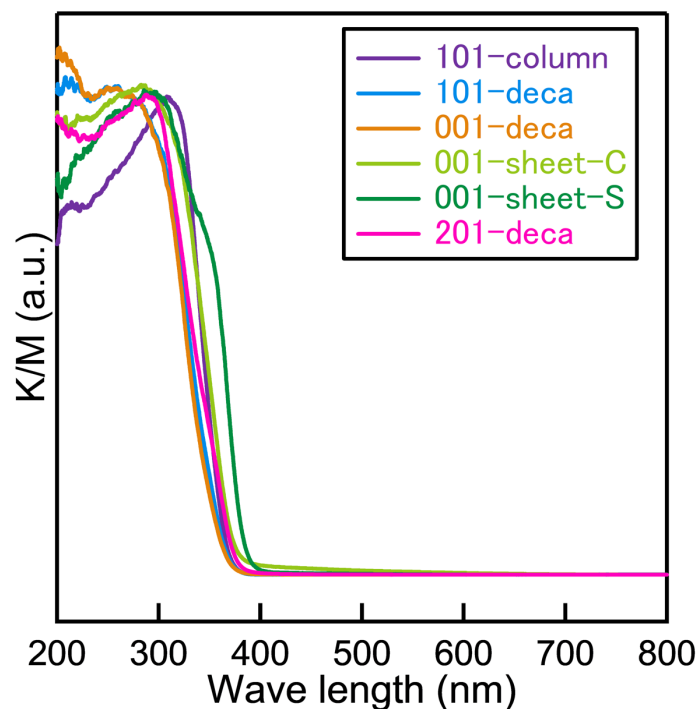


Figure S13 UV-vis spectra of TiO₂ NPs.

The absorption edges in UV-visible spectra for the TiO₂ NPs were located between 360 nm and 400 nm. Especially the adsorption edge of 001-sheet-S is located on the high wavelength side than other TiO₂ NPs. Therefore, the band gap energy of 001-sheet-S is smaller than other TiO₂ NPs. The variation for the band gap can be a sign of lattice defects, and therefore the existence of oxygen defects is predicted in 001-sheet-S.

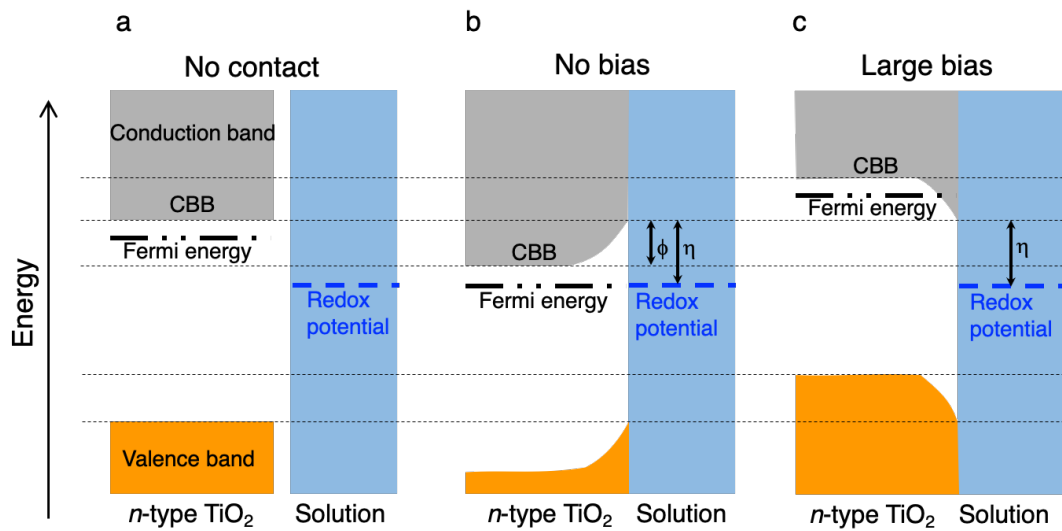


Figure S14 (a) Energy levels of *n*-type TiO₂ and the electrolyte solution without their contact and (b) with contact without or (c) under the bias potential. CBB, ϕ and η express conduction band bottom, built-in potential and reduction power (or overpotential), respectively.

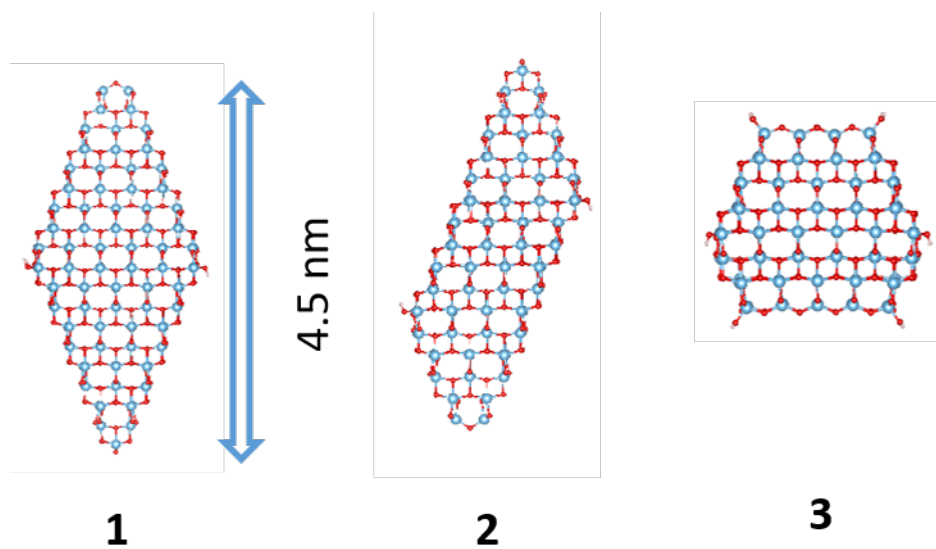


Figure S15 Geometry of nanoparticle models NP 1-3. Octahedral (**NP 1**), columnar (**NP 2**) and decahedral nanoparticles (**NP 3**).

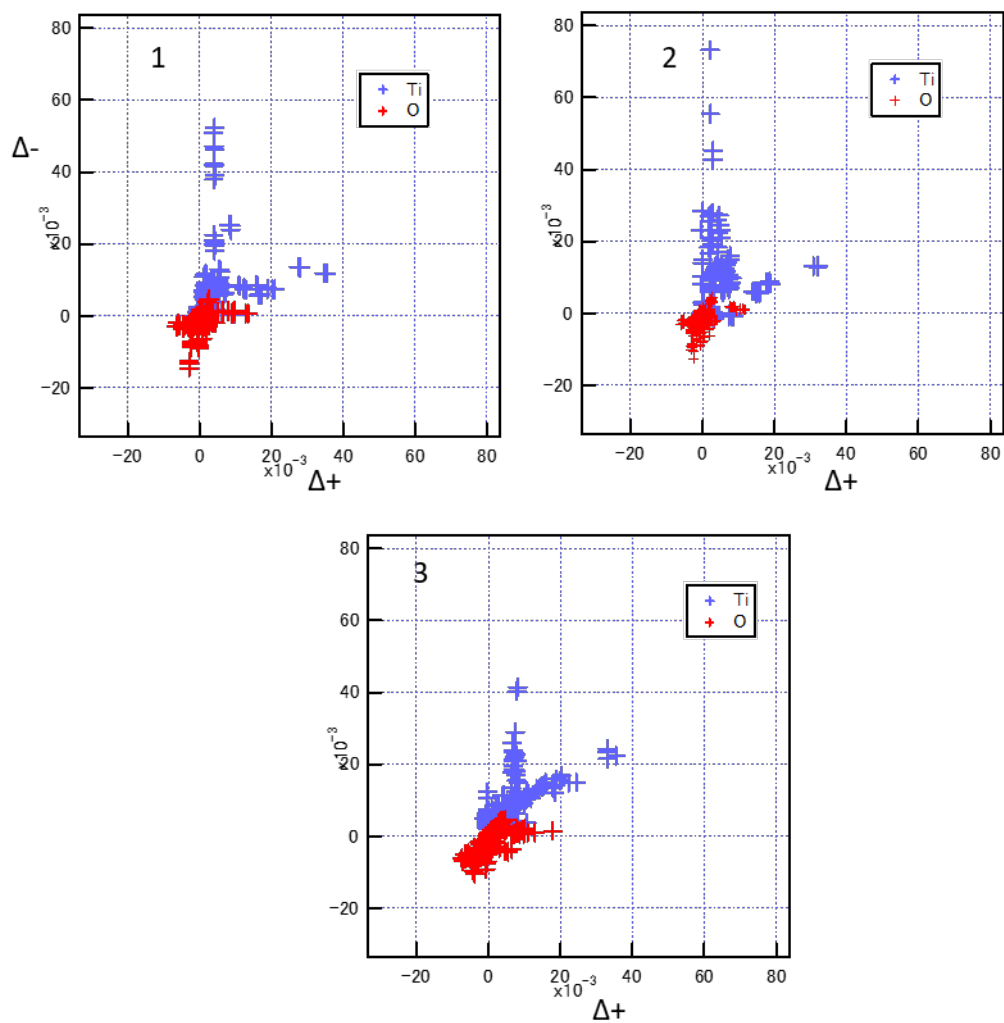


Figure S16. The extra negative charge vs positive charge ($\Delta-$ vs $\Delta+$) by element (Ti and O) in the particles **NP1-3** calculated from Mulliken charges.

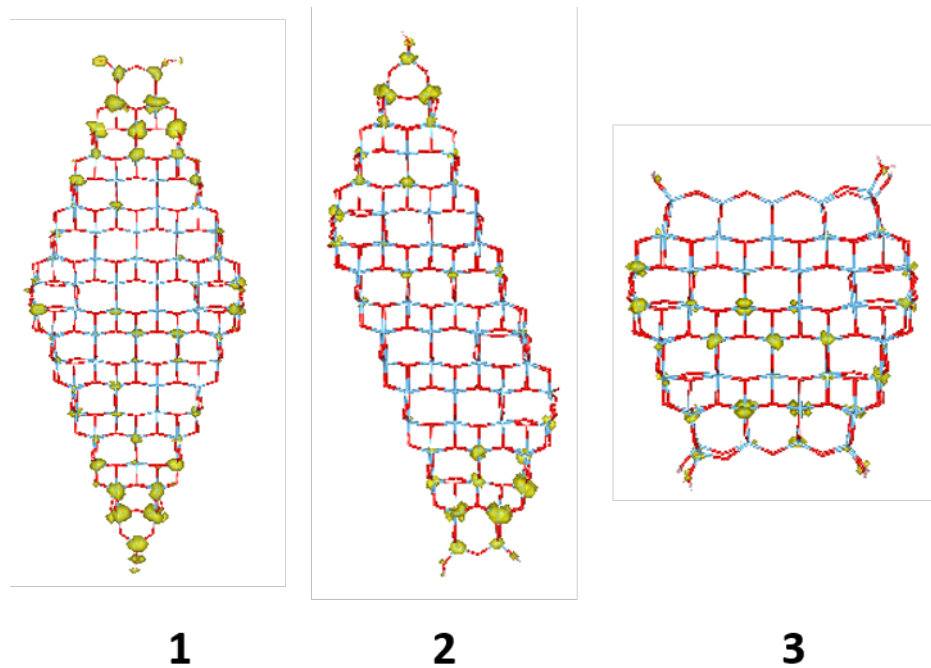


Figure S17 The extra negative charge density (yellow) in the reduced particles **NP1-3**.

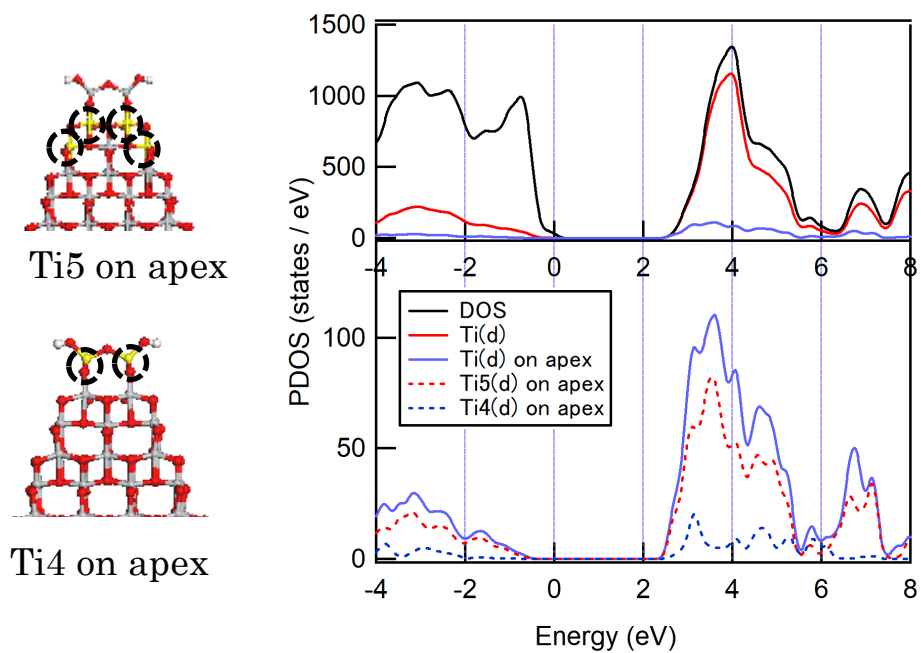


Figure S18 PDOS of nanoparticle model NP1: density of state (DOS), the d orbitals of all Ti atoms (Ti(d)), the d orbitals of Ti atoms on apexes with four coordination (Ti4(d)), five coordination (Ti5(d)).

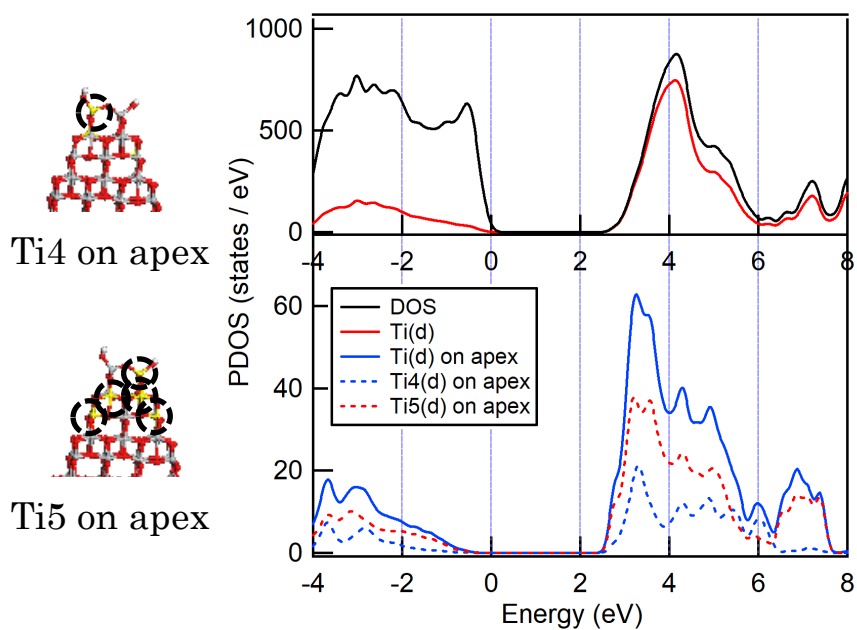


Figure S19 PDOS of nanoparticle model NP2: density of state (DOS), the d orbitals of all Ti atoms (Ti(d)), the d orbitals of Ti atoms on apexes with four coordination (Ti4(d)), five coordination (Ti5(d)).

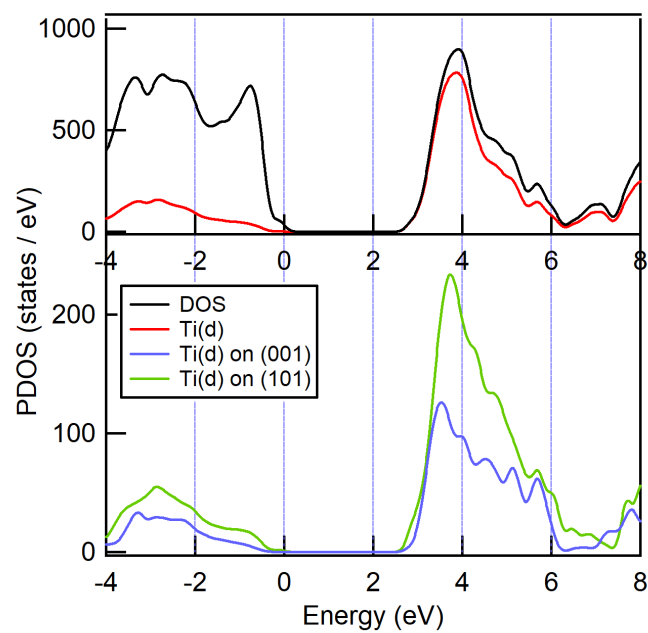


Figure S20 PDOS of nanoparticle model NP3: density of state (DOS), the *d* orbitals of all Ti atoms (Ti(*d*)), the *d* orbitals of Ti atoms on (001) surface and edges (Ti(*d*) on (001)), and (101) surface (Ti(*d*) on (101)).

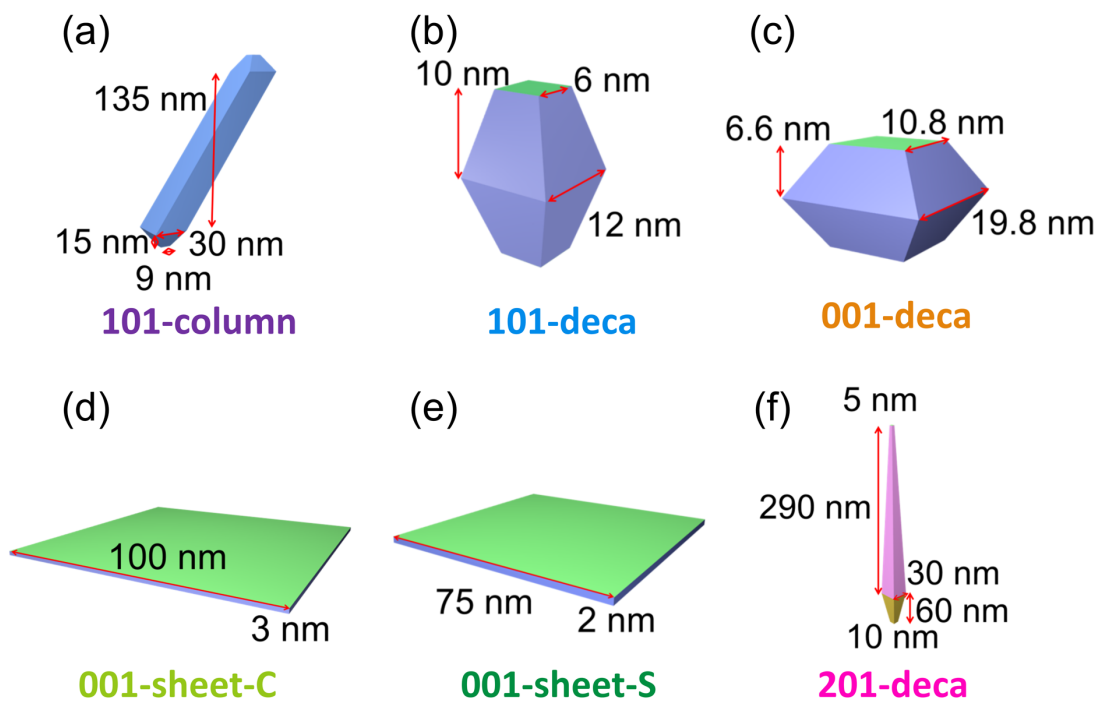


Figure S21 Model of TiO_2 NPs: (a) 101-column, (b) 101-deca, (c) 001-deca, (d) 001-sheet-C, (e) 001-sheet-S, (f) 201-deca.

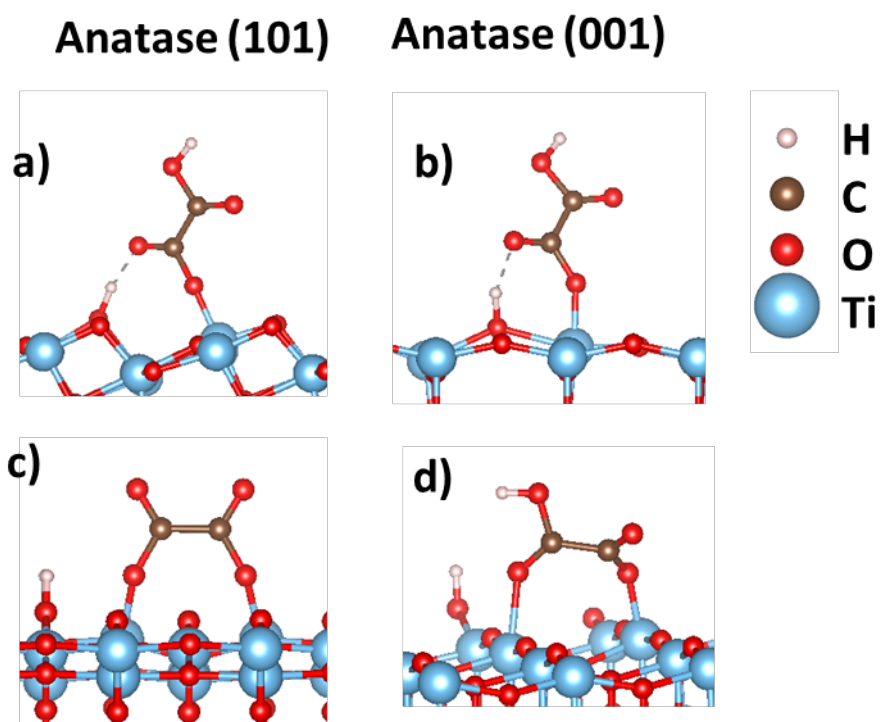


Figure S22 The geometry of oxalic acid absorbed dissociative way on (101) surface (*left: a, c*) and on (001) surface (*right: b, d*). Geometries with absorption trough a single carboxylic group are **a** and **b**, through both carboxylic groups: **c** and **d**. Corresponding absorption energies in are **a**: -129 kJ/mol, **b**: -218 kJ/mol, **c**: -80 kJ/mol, **d**: -380 kJ/mol.

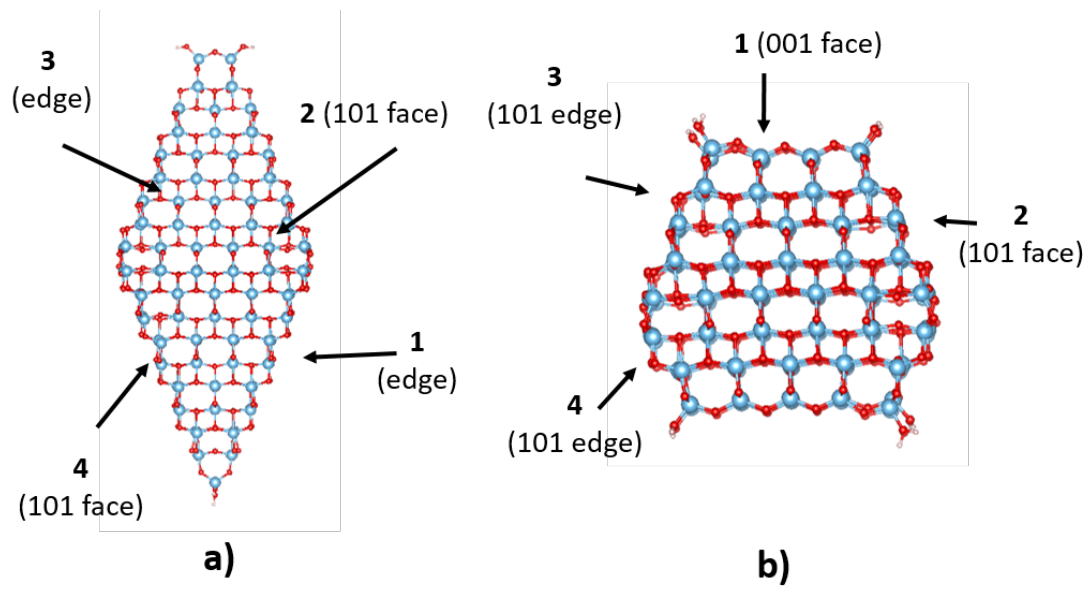


Figure S23. The studied absorption sites on NP1 (a) and NP3 (b).

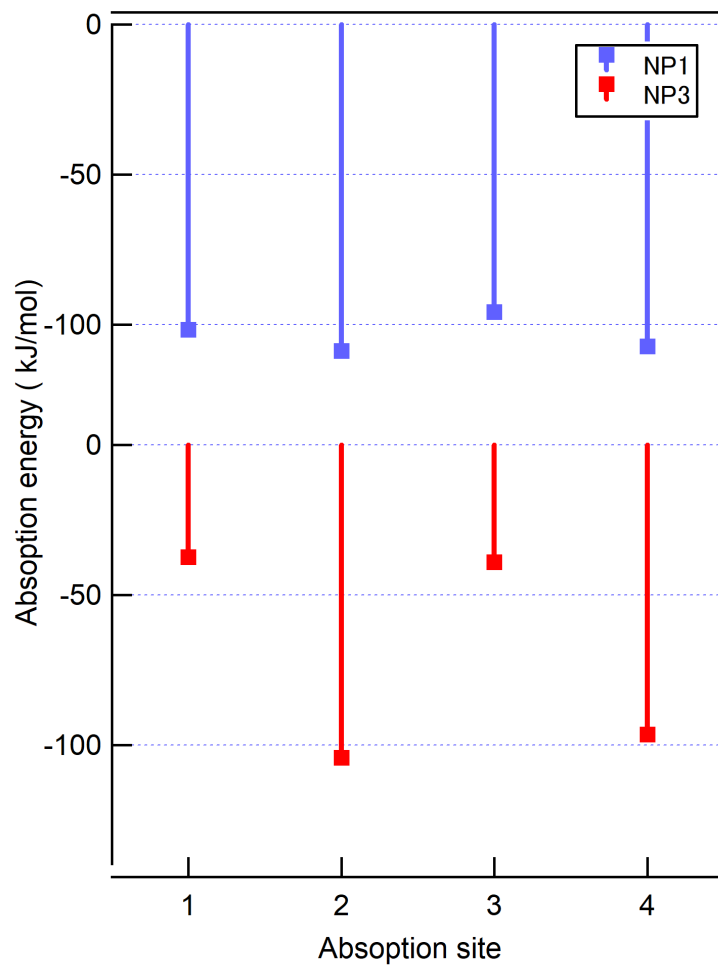


Figure S24 Absorption energies of oxalic acid for the absorption sites on **NP1** (*blue, top*) and **NP3** (*red, bottom*).

References

1. J. Chen, H. B. Yang, J. Miao, H.-Y. Wang, B. Liu, *J. Am. Chem. Soc.* 2014, **136**, 15310.
2. W. Q. Wu, H. S. Rao, Y. F. Xu, Y. F. Wang, C. Y. Su, D. B. Kuang, *Sci. Rep.* 2013, **3**, 1892.
3. Z. Wang, K. Lv, G. Wang, K. Deng, D. Tang, *Appl. Catal. B*, 2010, **100**, 378.
4. B. Wang, X. Zhang, H. Meng, H. Tao, *J. Nanosci. Nanotechnol.*, 2013, **13**, 356.
5. J. S. Chen, Y. L. Tan, C. M. Li, Y. L. Cheah, D. Luan, S. Madhavi, F. Y. C. Boey, L. A. Archer, X. W. Lou, *J. Am. Chem. Soc.*, 2010, **132**, 6124.
6. Z. Zhao, Z. Sun, H. Zhao, M. Zheng, P. Du, J. Zhao, H. Fan, *J. Mater. Chem.*, 2012, **22**, 21965.
7. H. B. Wu, J. S. Chen, X. W. David Lou, H. H. Hng, *Nanoscale*, 2011, **3**, 4082.
8. K. Kato, H. Tanaka, *Advances in Physics: X*, 2016, **1**, 55.
9. K. Kato, Y. Tanaka, M. Yamauchi, K. Ohara, T. Hatsui, *J. Synchrotron Rad.*, 2019, **26**, 762.
10. R. Watanabe, M. Yamauchi, M. Sadakiyo, R. Abe, T. Takeguchi, *Energ. Environ. Sci.*, 2015, **8**, 1456.
11. M. Yamauchi, S. Hata, H. Eguchi, S. Kitano, T. Fukushima, M. Higashi, M. Sadakiyo, K. Kato, *Catal. Sci. Technol.*, 2019, **9**, 6561.
12. B. Aradi, B. Hourahine and Th. Frauenheim, *J. Phys. Chem. A*, 2007, **111**, 5678.
13. M. Elstner, D. Porezag, G. Jungnickel, J. Elsner, M. Haugk, Th. Frauenheim, S. Suhai and G. Seifert, *Phys. Rev. B*, 1998, **58**, 7260.
14. G. Dolgonos, B. Aradi, N. H. Moreira, T. Frauenheim, *J. Chem. Theory Comput.*, 2010, **6**, 266.
15. H. J. Monkhorst, J. D. Pack, *Phys. Rev. B*, 1976, **13**, 5188.